Organic & Biomolecular Chemistry

Accepted Manuscript

This article can be cited before page numbers have been issued, to do this please use: N. Umekubo, A. Hashizume, H. Saito, S. Kato, C. Kanai, C. C. Gopalasingam, C. Gerle, H. Shigematsu, A. Yoshimori, K. Abe and S. Yokoshima, *Org. Biomol. Chem.*, 2025, DOI: 10.1039/D5OB01828E.

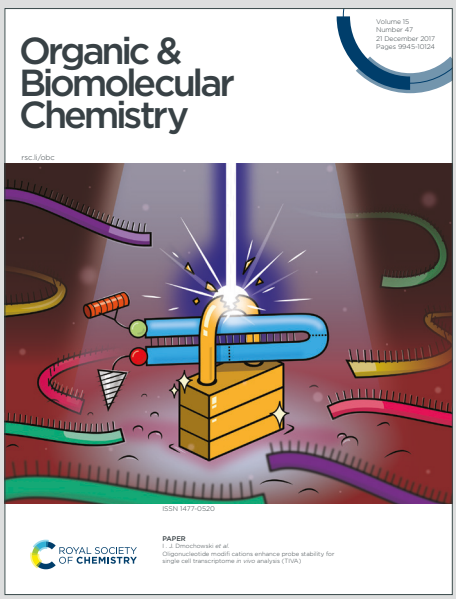

ROYAL SOCIETY OF CHEMISTRY

rsc.li/obc

View Article Online
DOI: 10.1039/D5OB01828E

ARTICLE

Design, Synthesis, and Structural Analysis of an Inhibitor of the Gastric Proton Pump with a Diaza-tricyclic Skeleton

Received 00th January 20xx,
Accepted 00th January 20xx

DOI: 10.1039/x0xx00000x

Nariyoshi Umekubo,[a] Airi Hashizume,[a] Haruki Saito,[b] Satoru Kato,[a] Chisato Kanai,[c] Chai C. Gopalasingam,[b,d] Christoph Gerle,[d] Hideki Shigematsu,[e] Atsushi Yoshimori,*[f] Kazuhiro Abe,*[b] Satoshi Yokoshima*[a]

The development of potent K⁺-competitive acid blockers (P-CABs) as inhibitors of acid gastric secretion attracts much research attention. In this study, the structure-guided design and enantioselective synthesis of P-CABs yielded a diaza-tricyclic compound with moderate inhibitory activity against the gastric proton pump. The eutomer was experimentally confirmed, consistent with pharmacophore predictions, and its binding mode to the gastric proton pump was elucidated via cryo-electron microscopy.

Introduction

K⁺-competitive acid blockers (P-CABs, Figure 1) are potent inhibitors of acid gastric secretion and as such are used for the treatment of acid-related gastric diseases such as peptic ulcers and gastroesophageal reflux disease. After the development of SCH28080 as the prototype of P-CAB, several molecules have been investigated, among which tegoprazan, revaprazan, and vonoprazan have reached clinical application in some Asian countries.

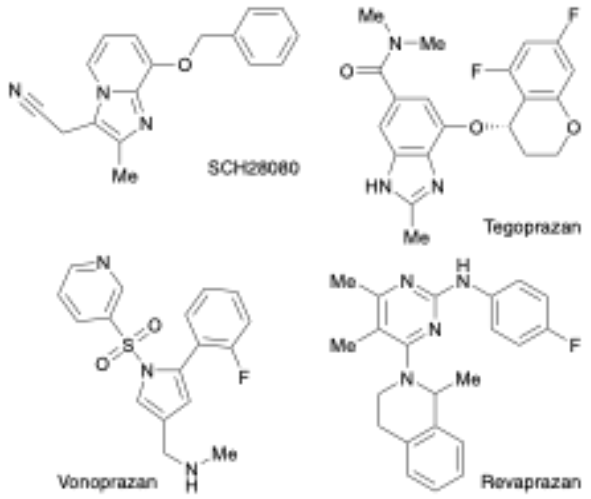

Figure 1 K⁺-competitive acid blockers

In 2023, we reported the development of novel P-CABs employing an approach combining cryo-electron microscopy (cryo-EM) for structure analysis, deep generative models for de novo drug design, and organic synthesis.[1] Thus, pharmacophores were defined in the drug-bound gastric proton pump structures,[2] and compounds satisfying the pharmacophores were designed in silico using our deep generative models "Deep Quartet." Several compounds were synthesized and evaluated for their inhibition activities in vitro. The binding poses of the compounds were analyzed via cryo-EM and fed back into the compound design. This approach allowed identifying DQ-18 as a potent P-CAB with a K_i value of 47.6 nM (Figure 2).

[a] Graduate School of Pharmaceutical Sciences, Nagoya University, Nagoya, Aichi 464-8601, Japan. E-mail: yokoshima.satoshi.v7@f.mail.nagoya-u.ac.jp
[b] Department of Chemistry, Faculty of Science, Hokkaido University, Sapporo, Japan. E-mail: kabe@sci.hokudai.ac.jp
[c] INTAGE Healthcare, Inc., 3-5-7, Kawaramachi Chuo-ku, Osaka 541-0048, Japan.
[d] RIKEN SPring-8 Center, 1-1-1 Kouto, Sayo, Hyogo 679-5148, Japan
[e] Japan Synchrotron Radiation Research Institute (JASRI), Spring-8, 1-1-1 Kouto, Sayo, Hyogo 679-5148, Japan
[f] Institute for Theoretical Medicine, Inc., 26-1, Muraoka-Higashi 2-chome, Fujisawa, Kanagawa 251-0012, Japan. yoshimori@itmol.com
Supplementary Information available. See DOI: 10.1039/x0xx00000x

View Article Online
DOI: 10.1039/D5OB01828E

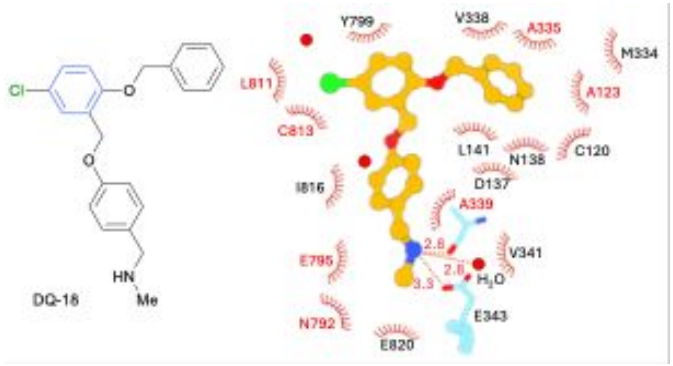

Figure 2 Structure and binding pose of DQ-18

DQ-18 has an *N*-methylamino group common to vonoprazan, which interacts in the gastric proton pump with the cation-binding site where three glutamates (Glu343, Glu795, and Glu820) are located. The benzene ring connecting to the *N*-methylamino group occupies the hydrophobic conduit of the gastric proton pump. Meanwhile, the benzene ring at the other terminal of DQ-18 occupies another hydrophobic region near the Ala123 residue. These three structural features, i.e., the *N*-methylamino group and two benzene rings, play important roles in the binding. We hypothesized that a novel P-CAB could be designed by replacing the central benzene ring (shown in blue, Figure 2) with a different core structure while preserving the three key features. Specifically, we aimed to design a rigid and three-dimensional skeleton because these two characteristics are essential in drug discovery. In particular, three-dimensional structures, which are built with sp^3 carbons, exhibit beneficial properties for drug discovery, such as high solubility, low promiscuity, and low CYP inhibitory activity.[3] The rigidity of the skeleton is also required because it allows the substituents to be fixed in specific positions.[4] Herein, we disclose the development of a novel P-CAB with a rigid and three-dimensional skeleton.

Results and discussion

Design and synthesis of P-CABs

To obtain a novel P-CAB, we designed various rigid and three-dimensional core skeletons by considering the size of the binding pocket and their synthetic accessibility. By attaching two substituents on the skeletons, candidate structures were generated and screened in silico. Among them, compound **1** was identified as a potent molecule with a diaza-tricyclic skeleton consisting of pyrrolidine, piperidine, and cyclopropane rings (Scheme 1).[5] To our surprise, the synthesis of the diaza-tricyclic skeleton was not previously reported, except as a partial structure of a pentacyclic aminal.[6] In addition, pharmacophore fitting of the enantiomers suggested that both can interact with the gastric proton pump, with a slight preference for one of them (vide infra). To verify this preference, we sought to obtain compound **1** in an optically active form by developing an asymmetric synthetic route for the core scaffold (Scheme 2).

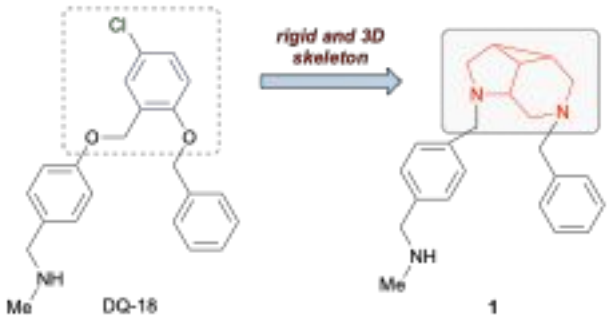

Scheme 1 Design of a K^+-competitive acid blocker.

The synthesis commenced with the copper-catalyzed enantioselective nitroaldol reaction of cinnamaldehyde (**2**) using chiral diamine **A** as the ligand,[7] which afforded the known alcohol **3** in 67% yield with an enantiomer ratio (er) of 96:4. Recrystallization from xylene improved the enantiopurity to 98.5:1.5. Reduction of the nitro group in **3** with zinc in acetic acid yielded aminoalcohol **4**, onto which a nosyl (Ns, 2-nitrobenzenesulfonyl) group was introduced.[8] Allylation of the resulting nosylamide **5** under basic conditions proceeded smoothly to give compound **6**. After replacing the Ns group with a *tert*-butoxycarbonyl (Boc) group, a tetrahydropyridine ring was constructed via ring-closing metathesis, affording **8a**.[9] A Mitsunobu reaction with nosylamide **9** furnished compound **10a**.[10] At this stage, the enantiomer ratio was confirmed via chiral HPLC, showing that partial racemization occurred (er = 91.5:8.5). In general, the Mitsunobu reaction of allylic alcohols proceeds predominantly via an S_N2 mechanism. However, allylic migration with anti-addition also occurred, leading to partial racemization.[11] The Ns group was then removed under standard conditions. The resulting secondary amine **11a** was converted into diazoacetamide **12a** in a two-step sequence involving bromoacetylation and a reaction with *N*,*N*′-ditosylhydrazine.[12] Direct cyclopropanation of **12a** via treatment with a rhodium catalyst did not produce the desired compound, most likely because the rhodium carbenoid generated in situ reacted with the benzene ring.[13] However, to our delight, heating in 1,2-dichloroethane (DCE) at 70°C promoted the intramolecular cycloaddition of the diazo moiety with the C–C double bond to form pyrazoline **13a**, which was then converted into the requisite cyclopropane **14a** by irradiating with blue LED light in the presence of an iridium complex.[13a, 14] Removal of the *tert*-butyldimethylsilyl group with tetra-*n*-butylammonium fluoride, followed by a Mitsunobu reaction with *N*-methyl-nosylamide, gave compound **16a**. After acidic cleavage of the Boc group, a benzyl group was introduced on the resulting secondary amine via reductive alkylation with benzaldehyde. Finally, removal of the Ns group and subsequent reduction of the lactam moiety with lithium aluminum hydride produced compound **1a**.

View Article Online
DOI: 10.1039/D5OB01828E

ARTICLE

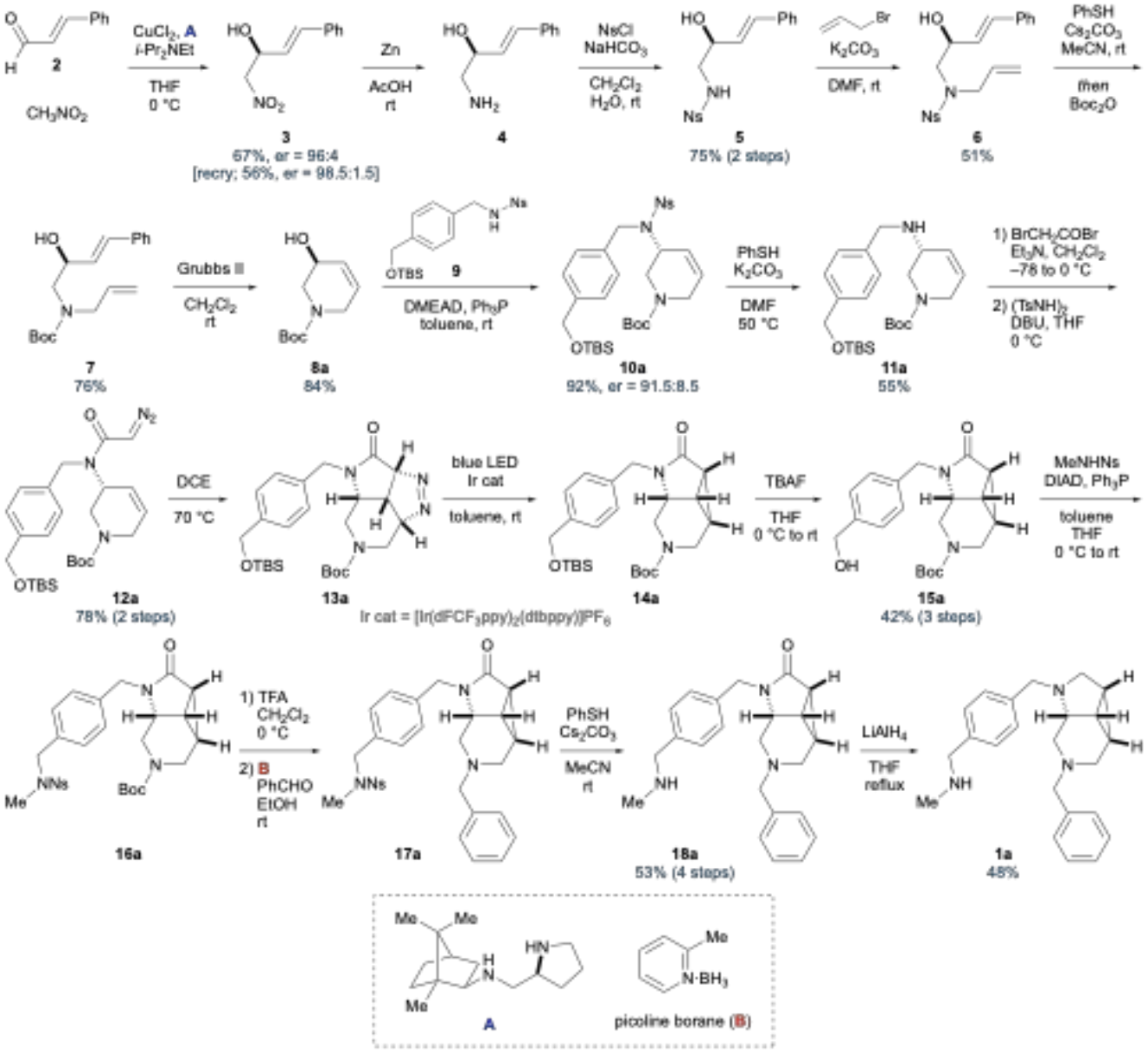

Scheme 2 Asymmetric Synthesis of Enantiomer **1a**.

For the preparation of the opposite enantiomer, we attempted the inversion of the configuration of **8a** via a Mitsunobu reaction (Scheme 3). Specifically, **8a** was treated with diethyl azodicarboxylate (DEAD), triphenylphosphine, and benzoic acid, giving benzoate **19**. Methanolysis of **19** under basic conditions afforded **8b**. After the Mitsunobu reaction with **9**, the enantiomer ratio was confirmed via chiral HPLC, which revealed the occurrence of partial racemization (er = 87:13). Using the same procedure, **10b** was converted into **1b**.

View Article Online
DOI: 10.1039/D5OB01828E

Scheme 3 Synthesis of the Opposite Enantiomer **1b**.

Biological evaluation and cryo-EM analysis

With both enantiomers in hand, we evaluated their potency by measuring the dose-dependence of ATPase activity inhibition using H^+,K^+-ATPase-enriched membrane fractions, according to previously reported protocols (Figure 3a).[1] Despite exhibiting lower IC_{50} values than the reference compound SCH28080 ($IC_{50,SCH}$ = 0.60 μM), compounds **1a** and **1b** inhibit the H^+,K^+-ATPase activity in a dose-dependent manner with IC_{50} values of 92.0 and 14.0 μM, respectively. The configuration of the more active enantiomer (eutomer, **1b**) is the same as that of the optical isomer that exhibited stronger binding in the pharmacophore fitting (Figure 3b).

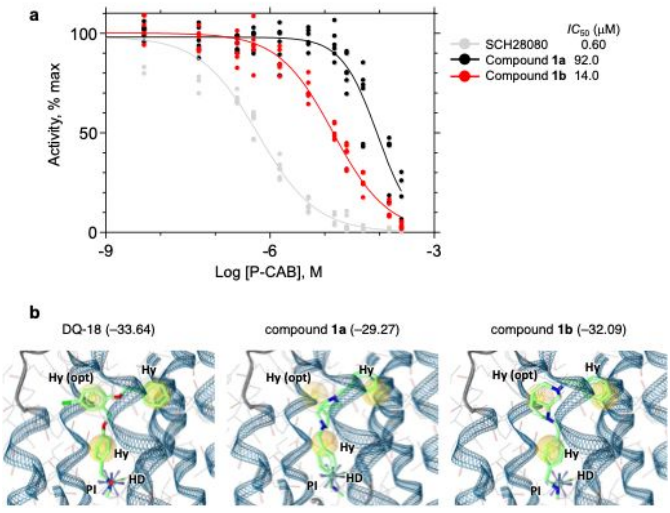

Figure 3 Inhibition potency and pharmacophore fitting of compounds **1a** and **1b**. **a** Dose-dependent inhibition of H^+,K^+-ATPase activity by **1a**, **1b**, and SCH28080 as a control. The data plotted represent each data point from three independent measurements with 12 different concentrations of P-CABs using membrane fractions purified from pig stomach. **b** Pharmacophore fitting between each compound and the gastric proton pump. The pharmacophore was constructed on the basis of the binding interactions between DQ-18 and the gastric proton pump (PDB: 8IJX). Yellow spheres indicate hydrophobic (Hy) features. A bluish sphere with spines and a green arrow indicates a positive ionization (PI) feature and a hydrogen bond donor (HD) feature, respectively. Hy opt is classified as an optional feature. While it is not essential, it can enhance the pharmacophore score when appropriately matched. Binding affinity scores (in kJ/mol) are shown in parentheses.

We also performed a cryo-EM analysis of H^+,K^+-ATPase bound to compound **1b** to verify its binding mode (Figure 4). The EM map analyzed at an overall resolution of 2.66 Å unambiguously resolved the densities corresponding to compound **1b** with surrounding water molecules and amino acids (Figure 4b). As expected according to the positions of the pharmacophore features set in Deep Quartet and the docking simulations (Figure 3b), compound **1b** is bound to the luminal-facing conduit in the transmembrane region of the gastric proton pump, which connects the cation-binding site (e.g., E343, E795, and E820) to the gastric luminal solution (Figure 4c). The cationic secondary amine moiety of **1b** is located close to the cation-binding site, suggesting a weak electrostatic interaction with the Glu343 side chain (3.9 Å). This characteristic is observed in DQ-related compounds and vonoprazan, faithfully reflecting the pharmacophore feature defined in the Deep Quartet calculation.[1] A hydrogen bond with the main chain carbonyl of Ala339 (2.9 Å) is also observed. These polar interactions may contribute to fixing the binding position of **1b** in the hydrophobic pocket. Apart from the abovementioned polar interactions, there are many van der Waals interactions with surrounding amino acids, including Val341 (3.4 Å), Glu795 (3.7 Å), Asn792 (3.5 Å), and Glu820 (3.4 Å) (Figure 4f). The two benzene rings are positioned to satisfy the defined pharmacophore features and thus engage in hydrophobic interactions with the snugly fitted binding pocket (Figure 4d,e). The core diaza-tricyclic skeleton of **1b** is juxtaposed to Tyr799 (Figure 4c). To our surprise, despite the bulkiness of this scaffold, it fits well within the binding pocket (Figure 4d,e). However, the π–π interaction that most P-CABs form with Y799 by placing an sp^2 functional group at this position is not expected for compound **1b**. This may be one of the reasons for its lower apparent affinity compared with DQ18 and other P-CABs. Interestingly, when compared with the DQ18-bound structure, the positions of Y799 and TM2 are displaced (Figure 4g). Owing to the presence of the bulky diaza-tricyclic skeleton, Y799 moves by 0.9 Å, and TM2, including Asn137 and Asn138, shifts by 0.7 Å, widening the binding pocket. This demonstrates that the relationship between the proton pump binding site and the inhibitor is not a simple lock-and-key model; instead, the compound binding induces small-scale conformational changes. Such induced fit was not observed with SCH28080, whose bicyclic imidazopyridine ring occupies the position of the diaza-tricyclic skeleton, suggesting the characteristic effect of this sp^3-rich, nonplanar, and bulky scaffold.

View Article Online
DOI: 10.1039/D5OB01828E

ARTICLE

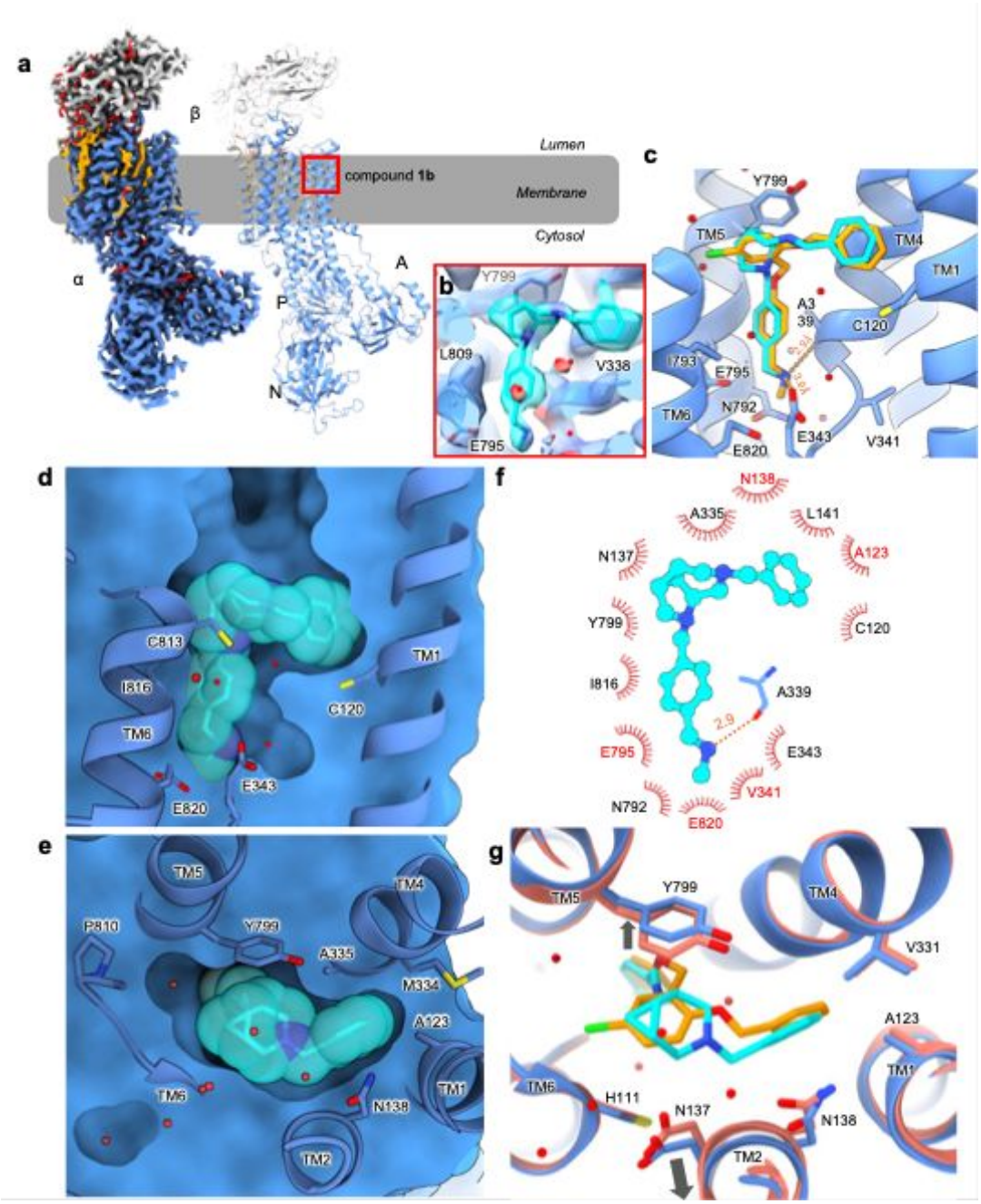

Figure 4 Cryo-EM (cryo-electron microscopy) structure of the gastric proton pump bound to compound **1b**. a, EM potential map (colored surface) and cartoon model of the gastric H^+,K^+-ATPase complexed with **1b** (α-subunit, blue; β-subunit, light gray; lipids, orange; water molecules, red). b, Close-up view of the binding site of compound **1b** indicated by the red box in a. The transparent blue surface represents the EM density map. c, Cartoon representation of the binding site of **1b** viewed parallel to the membrane plane with the luminal side up. Only several amino acids involved in the binding are displayed in stick representation. The structure of DQ-18 (orange) is superimposed on the binding structure of **1b** for comparison. Expected polar interactions within 3.9 Å are indicated by orange dotted lines. TM2 is omitted for clarity. d, e, Clipped cross sections of the binding site of **1b** viewed parallel to the membrane (d) or from the luminal side (e). Molecular surface (blue) of the gastric proton pump showing the dimension of the binding site that accommodates **1b** (cyan stick with transparent van der Waals spheres). TM helices and some of the key amino acids are shown in ribbon and stick representations. f, Schematic 2D representation of the binding pose of **1b**. Hydrophobic residues located within 3.9 Å from **1b** are shown, and those within 3.5 Å are highlighted in red. Expected polar interactions within 3.5 Å are indicated as orange dotted lines. g, Comparison of the binding site structure of the gastric proton pump bound to DQ-18 (gold and salmon red, PDB: 8IJX) with that

of **1b**. Arrows indicate displacement of Tyr799 (0.9 Å) and whole TM2 (0.7 Å) in the bound form of **1b** (blue and cyan) compared with the bound structure of DQ-18 (gold and salmon red).

View Article Online
DOI: 10.1039/D5OB01828E

Conclusions

We designed P-CABs based on the cryo-EM structure of the gastric proton pump bound to DQ-18, and pharmacophore fitting allowed identifying a potent candidate with a diaza-tricyclic skeleton consisting of pyrrolidine, piperidine, and cyclopropane rings. We established a synthetic route to the diaza-tricyclic skeleton via an enantioselective nitroaldol reaction, construction of the cyclopropane ring through a 1,3-dipolar cycloaddition of a diazo compound, and subsequent nitrogen extrusion from the resulting pyrazoline intermediate. Stereoinversion via a Mitsunobu reaction enabled the preparation of both enantiomers. Biological evaluation revealed that both enantiomers exhibited moderate inhibitory activity against the gastric proton pump, with compound **1b** being the more active enantiomer, as predicted by pharmacophore fitting. The binding features of compound **1b** to the gastric proton pump were elucidated via a cryo-EM analysis.

Author contributions

S.Y. designed the study with K.A., A.Y., and N.U. C.K. and A.Y. performed in-silico screening. N.U., A.H., S.K., and S.Y. synthesized the compounds. Ha.S. performed the ATPase assay. Ha.S. expressed and purified the protein. Ha.S. and K.A. performed the cryo-EM analysis with C.C.G, C.G., and Hi.S. Ha.S., C.C.G., and K.A. performed image processing, model building, and structural interpretations. S.Y., K.A., A.Y., and N.U. wrote the manuscript.

Conflicts of interest

There are no conflicts to declare.

Data availability

The data supporting this article have been included as part of the supplementary information. The structural data generated in this study have been deposited in the Protein Data Bank and EM Data Bank under accession codes 9VVO and EMD-65385.

Acknowledgements

This work was financially supported by JSPS KAKENHI (Grant Numbers JP23H02602, JP23K14321, JP24H01767, and JP24K01957); by the Research Support Project for Life Science and Drug Discovery [Basis for Supporting Innovative Drug Discovery and Life Science Research (BINDS)] from the Japan Agency for Medical Research and Development (AMED) under Grant Number JP25ama121044 (support number 4085) and JP25ama121001 to Masaki Yamamoto, C.G., C.C.G., and H.S.; and by JST CREST (Grant number JPMJCR22E4). Cryo-EM data are acquired using EM01CT of SPring-8 with approval of the Japan Synchrotron Radiation Research Institute (proposal number 2024B2519).

Notes and references

1 K. Abe, M. Ozako, M. Inukai, Y. Matsuyuki, S. Kitayama, C. Kanai, C. Nagai, C. C. Gopalasingam, C. Gerle, H. Shigematsu, N. Umekubo, S. Yokoshima and A. Yoshimori, *Commun. Biol.*, 2023, **6**, 956.
2 (a) K. Abe, K. Irie, H. Nakanishi, H. Suzuki and Y. Fujiyoshi, *Nature*, 2018, **556**, 214; (b) S. Tanaka, M. Morita, T. Yamagishi, H. V. Madapally, K. Hayashida, H. Khandelia, C. Gerle, H. Shigematsu, A. Oshima and K. Abe, *J. Med. Chem.*, 2022, **65**, 7843.
3 (a) F. Lovering, J. Bikker and C. Humblet, *J. Med. Chem.*, 2009, **52**, 6752; (b) F. Lovering, *MedChemComm*, 2013, **4**, 515.
4 A. D. G. Lawson, M. MacCoss and J. P. Heer, *J. Med. Chem.*, 2018, **61**, 4283.
5 Several skeletons have been identified as likely. Works on other skeletons are currently underway and will be reported in due course.
6 O. Tsuge, S. Kanemasa and S. Takenaka, *Bull. Chem. Soc. Jpn.*, 1983, **56**, 2073.
7 Y. Zhou, J. Dong, F. Zhang and Y. Gong, *J. Org. Chem.*, 2011, **76**, 588.
8 (a) T. Fukuyama, C.-K. Jow and M. Cheung, *Tetrahedron Lett.*, 1995, **36**, 6373; (b) T. Kan and T. Fukuyama, *Chem. Commun.*, 2004, 353.
9 (a) C. Lecourt, S. Dhambri, L. Allievi, Y. Sanogo, N. Zeghbib, R. Ben Othman, M. I. Lannou, G. Sorin and J. Ardisson, *Nat. Prod. Rep.*, 2018, **35**, 105; (b) M. Yu, S. Lou and F. Gonzalez-Bobes, *Org. Process Res. Dev.*, 2018, **22**, 918; (c) E. J. Groso and C. S. Schindler, *Synthesis*, 2019, **51**, 1100.
10 (a) O. Mitsunobu, *Synthesis*, 1981, **1981**, 1; (b) K. C. K. Swamy, N. N. B. Kumar, E. Balaraman and K. V. P. P. Kumar, *Chem. Rev.*, 2009, **109**, 2551; (c) S. Fletcher, *Org. Chem. Frontiers*, 2015, **2**, 739.
11 B. K. Shull, T. Sakai, J. B. Nichols and M. Koreeda, *J. Org. Chem.*, 1997, **62**, 8294.
12 T. Toma, J. Shimokawa and T. Fukuyama, *Org. Lett.*, 2007, **9**, 3195.
13 (a) Y. Ohfune, T. Demura, S. Iwama, H. Matsuda, K. Namba, K. Shimamoto and T. Shinada, *Tetrahedron Lett.*, 2003, **44**, 5431; (b) T. Miura, Y. Funakoshi and M. Murakami, *J. Am. Chem. Soc.*, 2014, **136**, 2272.
14 M. J. R. Richter, F. J. Zécri, K. Briner and S. L. Schreiber, *Angew. Chem. Int. Ed.*, 2022, **61**, e202203221.

View Article Online
DOI: 10.1039/D5OB01828E

Data availability

The data supporting this article have been included as part of the supplementary information. The structural data generated in this study have been deposited in the Protein Data Bank and EM Data Bank under accession codes 9VVO and EMD-65385.